Cancer-associated fibroblasts suppress SOX2-induced dysplasia in a lung squamous cancer coculture

Shuang Chen[a,1], Andreas Giannakou[a,1], Sarah Wyman[a], Janet Gruzas[a], Jonathon Golas[a], Wenyan Zhong[a], Christine Loreth[a], Latha Sridharan[a], Ting-Ting Yamin[a], Marc Damelin[a], and Kenneth G. Geles[a,2]

[a]Oncology R&D Group, Pfizer Worldwide Research and Development, Pearl River, NY 10965

Tumorigenesis depends on intricate interactions between genetically altered tumor cells and their surrounding microenvironment. While oncogenic drivers in lung squamous carcinoma (LUSC) have been described, the role of stroma in modulating tissue architecture, particularly cell polarity, remains unclear. Here, we report the establishment of a 3D coculture system of LUSC epithelial cells with cancer-associated fibroblasts (CAFs) and extracellular matrix that together capture key components of the tumor microenvironment (TME). Single LUSC epithelial cells develop into acinar-like structures with 0.02% efficiency, and addition of CAFs provides proper tumor–stromal interactions within an appropriate 3D architectural context. Using this model, we recapitulate key pathological changes during tumorigenesis, from hyperplasia to dysplasia and eventually invasion, in malignant LUSC spheroids that undergo phenotypic switching in response to cell intrinsic and extrinsic changes. Overexpression of SOX2 is sufficient to mediate the transition from hyperplasia to dysplasia in LUSC spheroids, while the presence of CAFs makes them invasive. Unexpectedly, CAFs suppress the activity of high SOX2 levels, restore hyperplasia, and enhance the formation of acinar-like structures. Taken together, these observations suggest that stromal factors can override cell intrinsic oncogenic changes in determining the disease phenotype, thus providing fundamental evidence for the existence of dynamic reciprocity between the nucleus and the TME of LUSC.

SOX2 | acinar morphogenesis | lung cancer | cancer-associated fibroblasts | 3D culture

L ung development is orchestrated through intricate epithelial–mesenchymal cross-talk that drives early events in morphogenesis such as specification, budding, and branching, as well as the final stages of postnatal lung alveologenesis (1, 2). Recent studies have demonstrated that key signaling pathways such as Wnt/β-catenin, Notch, Hedgehog, and fibroblast growth factor signaling are important mediators of this process (3). These signaling pathways regulate the expression of key factors in the lung epithelium, such as SOX2/SOX9 and NKX2-1 (TTF1), to determine the lineage identity and cell fate of lung progenitors. Epithelial–mesenchymal cross-talk in lung cancer also has become the subject of intense interest due to recent findings that many of these intercellular signaling pathways and key factors are aberrantly regulated during lung tumorigenesis (4–6).

Squamous cell carcinoma of the lung (LUSC) is the second most common type of non-small cell lung cancer (NSCLC) after lung adenocarcinoma (LUAD), comprising ∼30% of all lung cancer (7–9). Both LUSC and LUAD ranked top in their mutation load among various cancer types, but the molecular abnormalities associated with the two subtypes are distinct (8, 10). For instance, the transcription factor SOX2 has been identified as a lineage-specific oncogene in LUSC (4), whereas LUAD tumorigenesis often depends on the expression of NKX2-1 (TTF1) (11). However, accumulating evidence has made it clear that tumorigenesis is not a cell-autonomous process but relies on dynamic and reciprocal interactions between the mutant tumor cells and their surrounding tumor microenvironment (TME) (12, 13). Most LUSC tumors are characterized by a

significant desmoplastic/fibrotic component in the TME at the time of diagnosis (14). In these tumors, extracellular matrix (ECM) organization is often altered due to increased deposition and posttranslational modifications of ECM proteins while cancer-associated fibroblasts (CAFs) accumulate closely around cancer nests. CAFs are known to be responsible for the deposition/modification of the ECM proteins as well as secretion of growth factors and chemokines (15, 16). These events contribute to changes in both the biochemical and biomechanical properties of the ECM and, in turn, affect tumor–TME interactions (17, 18). How changes in tumor cell–TME interaction influence cancer progression and aggressiveness in LUSC remains unclear.

Investigation of tumor cell–TME interactions could be greatly facilitated by models that mimic human disease on both the genotypic and phenotypic levels. Three-dimensional cultures represent an important means to study the impact of tumor cell–TME interactions on specific aspects of neoplastic phenotypes. This has been most prominently demonstrated using mammary epithelial cells, such as MCF-10A, that are seeded as single cells in basement membrane matrix derived from the murine Englebreth–Holm–Swarm sarcoma (Matrigel) and have the capacity to form acinar-like structures that parallel the complex organization of native tissue architectures with respect to apical–basal

polarity, cell–cell contacts, and cell–ECM adhesion (19). Malignant mammary epithelial cells, on the other hand, form unorganized structures accompanied by uncontrolled growth. Notably, altering the cell–ECM interaction could revert an unorganized structure back into an acinar phenotype, indicating that the phenotype of malignant breast cancer cells is plastic and regulated by cell–ECM interactions (20–23). Similar to mammary epithelial cells, human bronchial epithelial cells (HBEC) have the capacity to self-organize into acinar-like structures in 3D cultures (24). Nevertheless, due to the high level of genetic complexity, at least five oncogene/tumor suppressor changes are needed to transform HBEC cells into LUAD, and the combination for LUSC transformation has yet to be identified (25, 26).

Here, we report the establishment of a 3D coculture model that recapitulates key features of tissue architecture during LUSC progression as well as the dynamic interactions between LUSC cells and components of the TME, including the ECM and CAFs. Specifically, we demonstrate that a primary cell culture known as TUM622, which was generated from an LUSC patient-derived xenograft (PDX), forms acinar-like structures with apical–basal polarity when seeded in a basement membrane matrix, despite its malignant origin. These hollow acini are hyperplastic, but they have the potential to become dysplastic when SOX2 is overexpressed and invasive upon coculture with CAFs. These phenotypic changes recapitulate key stages in LUSC progression, from hyperplasia to dysplasia and eventually invasion (27). Unexpectedly, CAFs suppress the action of overexpressed SOX2 and restore hyperplasia, indicating that components in the TME could override cell-intrinsic oncogenic changes in determining the disease phenotype. Together, these data suggest that the interaction between the TME and tumor cells is a critical determinant of tumorigenesis in LUSC and represent an important opportunity for therapeutic intervention.

Results

TUM622 Cells Form Hyperplastic Acinar-Like Structures Composed of Polarized Cells. To establish a culture that would enable mechanistic study of tumor–TME interplay in a structurally appropriate context, we screened primary NSCLC cell cultures that could recapitulate key features of lung epithelium architecture when seeded in basement membrane matrix (see *Materials and Methods*). Specifically, primary human NSCLC cell cultures were embedded as single cells ($\leq$6,500 cells per 100 μL) in growth factor-reduced Matrigel and cultured with serum-free (SF) medium. The four primary cell cultures (TUM622, TUM426, TUM449, and TUM110) were previously established directly from either human NSCLC tumors or the corresponding PDX (28–30) (see also *SI Appendix*, Fig. S1*A*). Two serum-established NSCLC cell lines and two immortalized bronchial epithelial cell lines are included for comparison. Interestingly, while all other cell lines examined formed solid spheroids composed of homogenous round cells or concentric layers of cells, TUM622 gave rise to acinar-like structures (henceforth referred to as TUM622 acini) with a monolayer of cells surrounding a hollow lumen, similar in appearance to the acini that arise from other glandular epithelial cells such as MCF-10A (19) (Fig. 1*A*). Immunostaining showed that TUM622 cells uniformly express LUSC marker cytokeratin 5 (KRT5) and p63 (encoded by *TP63*), but not LUAD marker TTF1, confirming their squamous identity (*SI Appendix*, Fig. S1*B*). A time course experiment showed that the hollow lumen in TUM622 acini starts to form around day 5, becomes apparent around day 7, and remains hollow thereafter (Fig. 1*B* and *SI Appendix*, Fig. S1*C*). Fluorescent staining with live/dead markers (calcein/ethidium bromide) in TUM622 acini revealed that only a few cells are detached from the monolayer at any given time point and these cells are undergoing apoptosis (Fig. 1*B*, *Bottom*). This is in contrast with MCF-10A acini which first form as solid
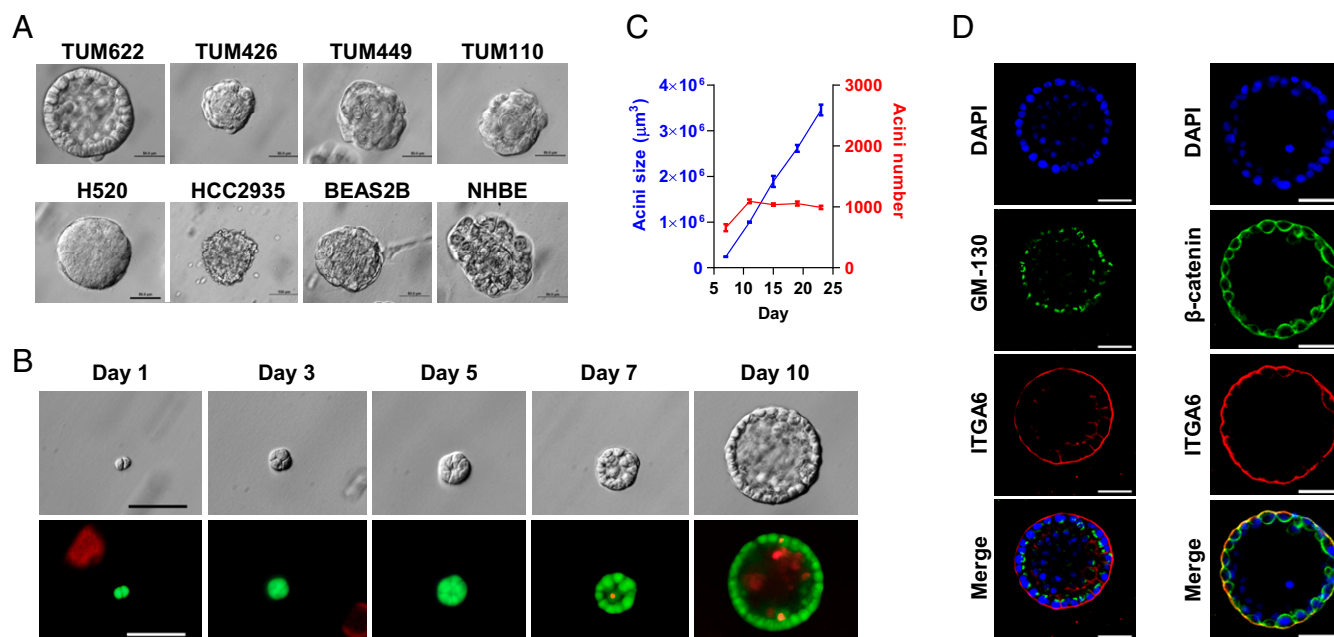
Fig. 1. TUM622 is capable of forming acinar-like structures in 3D ECM. (*A*) Representative bright-field images of spheroids derived from single NSCLC cells in 3D ECM culture between days 8 and 12. (*Top*) Cell lines (TUM622, TUM426, TUM449, and TUM110) are derived from either patient tumors or the corresponding PDX. (*Bottom*) Established cell lines of LUSC (H520), LUAD (HCC2935), and immortalized bronchial epithelial cells (BEAS2B and NHBE). (Scale bars, 50 μm.) (*B*) Time course images of TUM622 cell cultured in Matrigel over a 10-d period. (*Top*) Bright-field images. (*Bottom*) Green is calcein, marking live cells; red is ethidium bromide, marking dead cells. (Scale bars, 100 μm.) (*C*) Quantification of acini number (right y axis, red) and average size of acini (left y axis, blue) plated in triplicate in a 24-well plate over 23 d in culture. Error bars represent SD. (*D*) (*Left*) Immunofluorescence of TUM622 acini stained with apical–basal cell polarity markers Golgi enzyme GM130 (green, apical) and ITGA6 (CD49f, basal, red), (*Right*) in comparison with β-catenin staining (green). (Scale bars, 50 μm.)

spheroids with an inner core of cells that later undergo apoptosis en masse to create the lumen.

Tumor spheroids formed from cancer epithelial cells are often characterized by uncontrolled growth and lack of proper polarity (19). We then examined these two attributes in TUM622 acini by bright-field and fluorescent imaging. Results showed that TUM622 acini continued to increase in size even after 3 wk in culture (Fig. 1C). To further confirm that this increase in acini size is due to cell proliferation, we quantified the number of nuclei in DAPI-stained TUM622 acini at days 5, 10, and 15 (n = 5 for each time point). Results showed that the average cell number per acinus increases over time and correlates with that of acinar size (*SI Appendix*, Fig. S1 *D* and *E*). Aside from their malignant origin, TUM622 acini appear to display proper apical–basal cell polarity as evidenced by the basal expression of ITGA6 (CD49f) and apical localization of cis-Golgi enzyme GM-130 (GOLGA2). In comparison, β-catenin appears to be distributed throughout the cell membrane (Fig. 1D).

Together, these data showed that the LUSC PDX-derived TUM622 cells could form polarized yet non–growth-arrested acinar-like structures in 3D. This property provided a unique opportunity to investigate how cell intrinsic and extrinsic changes affect tumor growth and tissue architecture in a malignant background of LUSC.

TUM622 Acini Retain the Heterogeneity and Architecture of the Original PDX. Under the culture condition we used, only a small percent of TUM622 cells are acinar-forming, while the rest of the cells stop proliferating or undergo cell death shortly after plating. By limiting dilution assay (LDA) (31, 32), we estimated that 1 in 5,884 TUM622 cells (<0.02%) is capable of generating an acinar-like structure (Fig. 2A and *SI Appendix*, Fig. S2A). Although rare, these cells are capable of self-renewal. TUM622 acini could be dissociated and replated in 3D ECM and still be able to form similar numbers of acinar-like structures for multiple passages (Fig. 2B and *SI Appendix*, Fig. S2B). However, the observation that the acini number does not increase greatly between 3D serial passages suggests that each TUM622 acinus is not a simple expansion of acinar-forming cells (AFCs). To determine whether TUM622 acini remain malignant after subclonal selection in 3D culture, we embedded TUM622 acini s.c. into immunocompromised nude mice and measured tumor take and growth (*SI Appendix, Supplemental Methods*). Results showed that tumors were initiated in 100% (10/10) of the mice and continuously grew during the time period measured, confirming that they remain malignant after subclonal selection (Fig. 2C). We further characterized acini by immunofluorescent staining of markers, including CXCR4 (cancer stem cell/EMT/metastasis), SOX2 [embryonic stem (ES) cell/lung basal cell progenitor/lineage
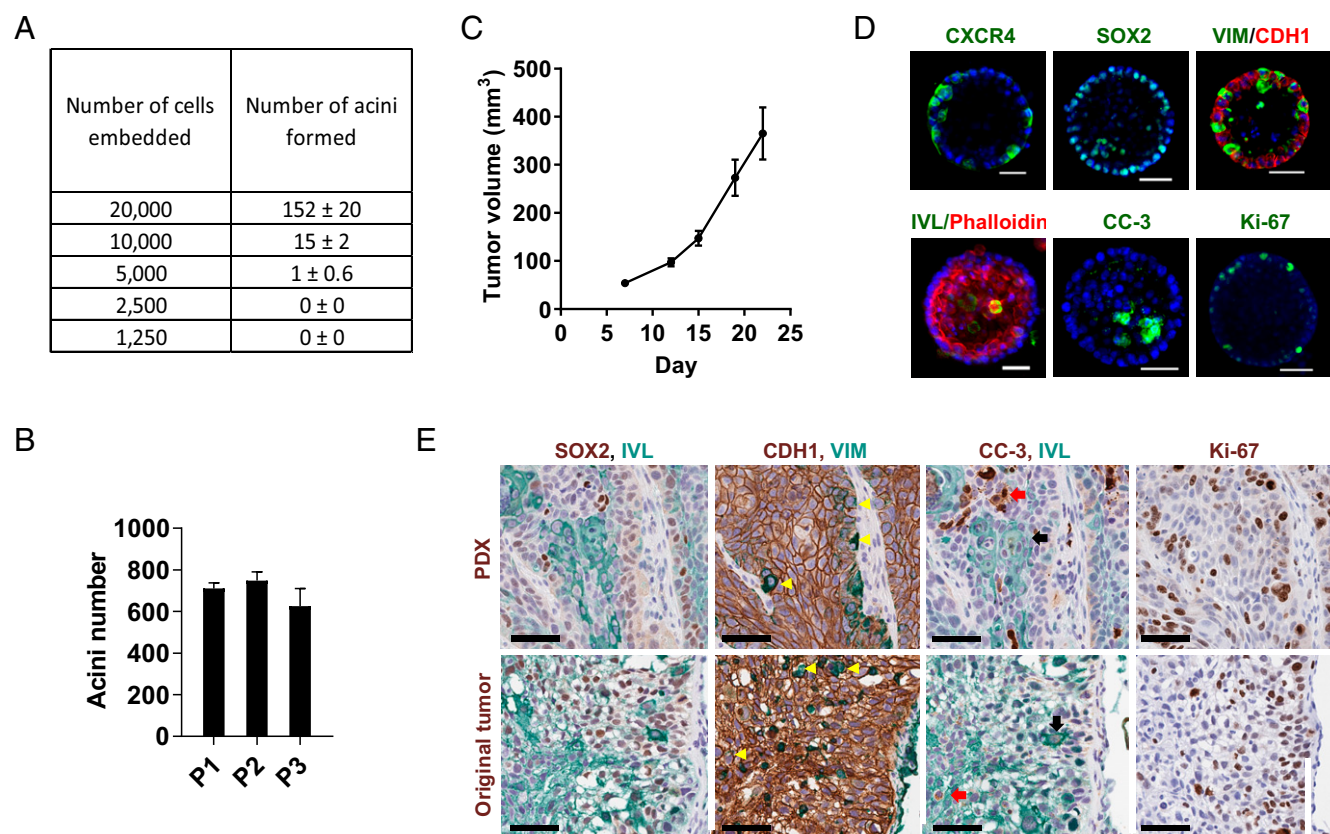
Fig. 2. Cells from TUM622 acini are capable of self-renewal and recapitulate the intratumoral heterogeneity observed in the PDX model and original human tumor. (*A*) Quantification of acinar-like structures formed in an LDA. Each seeding density is plated in triplicate. (*B*) Quantification of acini formed from three serial passages of TUM622 acini in Matrigel. Each passage is plated in triplicate. Error bars represent SD. (*C*) Quantification of in vivo growth of s.c. injected TUM622 acini; x axis represents days after injection, and y axis represents tumor volume (cubic millimeters). Error bars represent SEM. (*D*) Antibody staining of acini with markers of stem/progenitor cells (CXCR4 and SOX2), mesenchyme (Vimentin), epithelial differentiation (Involucrin), apoptosis (CC-3), and proliferation (Ki-67) in green; DAPI (blue), and CDH1 and Phalloidin (red). (Scale bars, 50 μm.) (*E*) Immunohistochemistry staining on sequential sections of TUM622 PDX and the human tumor from which it is derived. Magnification: 40×. Yellow arrow heads point to Vimentin and E-Cadherin double-positive cells. Red arrows point to cells undergoing apoptosis (CC-3–positive), and black arrows point to adjacent Involucrin positive cells that are negative for CC-3. (Scale bars, 60 μm.)

survival oncogene], Vimentin (mesenchyme), Involucrin (epithelial differentiation), Ki-67 (proliferation), and cleaved caspase-3 (CC-3, apoptosis) (Fig. 2D and *SI Appendix*, Fig. S2C). Results showed that the acini generated by the self-renewing AFCs are actually composed of a heterogeneous mixture of stem-like, differentiated, proliferative, and apoptotic cells, with only some but not all cells expressing any one of the markers tested. Markers such as CXCR4 and Vimentin also showed heterogeneous expression in 2D culture (*SI Appendix*, Fig. S2D). Notably, Involucrin and CC-3 are only detected when cells become detached from the monolayer and enter the lumen, similar to what is observed in MCF-10A acini. This observation indicates that contact with the ECM is important to maintain survival and prevent terminal differentiation of TUM622 cells.

To understand whether the heterogeneity observed in TUM622 acini mirrors that of the original tumor from which it was derived, we performed immunohistochemistry staining on the corresponding PDX as well as the original human tumor. Results showed that, while the majority of cancer epithelial cells are positive for E-Cadherin (CDH1), only a subpopulation of epithelial cells expresses SOX2, Involucrin, Vimentin, or Ki-67 in both the PDX and the original human tumor (Fig. 2E). Interestingly, in both the 3D and PDX models, SOX2-positive, Vimentin-positive, and Ki-67 −positive cells are mostly found to be on the periphery of cancer nests, whereas Involucrin-positive cells are farther away from the stromal cells and are located toward the center of the nests, highlighting the resemblance of their 3D architecture. In addition, we identified E-Cadherin and Vimentin double-positive cells in all samples examined, although the frequency of such cells is much higher in 3D culture and the PDX model compared with the patient sample. This heterogeneous expression pattern is not unique to TUM622 and could be identified in an additional human patient sample (*SI Appendix*, Fig. S2E).

In summary, these data suggest that TUM622 contains a subpopulation of cells with the ability to both self-renew and generate diverse progeny, some of which possess terminal lineage differentiation potential. Importantly, the acini derived from these cells recapitulate many aspects of the heterogeneity and architecture of the PDX model and human tumors.

Stem Cell and Developmental Pathway Genes Are Enriched in TUM622 3D Culture.
To gain a better understanding of the cell intrinsic mechanisms regulating TUM622 acinar morphogenesis in three dimensions, we performed transcriptional profiling of TUM622 cells collected from 2D and 3D cultures. Briefly, mRNA was purified from live epithelial cells harvested by FACS in three biological replicates per culturing condition and then used for gene expression profiling with the human U133A microarray. We identified genes that vary more than 1.5-fold with reproducible changes among the biological replicates ($P < 0.05$) and found a total of 9,227 genes differentially expressed, indicating that changing culture conditions from 2D to 3D exerts a major influence on gene expression in TUM622 cells (Dataset S1). To explore which of the annotated pathways and functional groups of genes are enriched in three dimensions, we employed Gene Set Enrichment Analysis (GSEA) and identified a total of 699 gene sets that are up-regulated in 3D culture [false discovery rate (FDR) < 0.25] (Dataset S2). Interestingly, these data include a large number of gene sets related to oncogenesis as well as genes and pathways involved in normal lung development, such as canonical Wnt, Notch, and Hedgehog signaling pathways, ES cell genes, and biological processes regulating acinar morphogenesis and polarity, as well as disease prognosis (Dataset S3). To identify the most significant gene sets, we applied a more stringent cutoff of FDR < 0.05 and a normalized enrichment score of >1.8 and found that the Wnt pathway, ES genes, polarity/acinar morphogenesis, and factors associated with poor prognosis are significantly enriched, while Notch and Hedgehog pathways are not (Fig. 3).

To functionally validate these results, we first tested whether the Wnt pathway regulates TUM622 acinar morphogenesis by measuring the dose–response of developing TUM622 acini treated with a small-molecule agonist (CHIR99021) and antagonist (IWR-1) of canonical Wnt signaling. Results showed that inhibition of Wnt abrogated acinar morphogenesis while activation of Wnt signaling disturbed acinar polarity leading to the loss of a hollow lumen. In contrast, inhibition of Notch signaling, which was not significantly enriched in the GSEA, did not affect acinar morphogenesis of TUM622 cells (*SI Appendix*, Fig. S3 A–C). Together, these data indicate that the process of TUM622 acinar morphogenesis is sensitive to perturbation of Wnt signaling.

We next examined the ES cell signature that is enriched in 3D culture. By qRT-PCR, we found that the expression level of SOX2, OCT4 (POU5F1), and NANOG are up-regulated in 3D compared with 2D culture, while KLF4 and c-MYC are largely unchanged (*SI Appendix*, Fig. S3D). The expression of SOX2 is higher than that of OCT4 or NANOG in both 2D and 3D cultures, and the up-regulation of SOX2 in 3D culture is further confirmed at the protein level (*SI Appendix*, Fig. S3E). To determine whether SOX2 has a functional role during TUM622 acinar morphogenesis, we performed loss-of-function studies of SOX2 by siRNA transfection. Data showed that reducing SOX2 in TUM622 cells inhibited acinar morphogenesis in TUM622 cells as well as other NSCLC cell lines while having minimal effect on cell viability (*SI Appendix*, Fig. S3 F–H).

Collectively, these data suggest that the Wnt signaling pathway and stem cell factor SOX2, which play a role in normal lung development, are involved in acinar morphogenesis of TUM622 cells in three dimensions. The enrichment in gene sets related to poor prognosis is consistent with 3D culture selecting for cells with higher tumorigenic potential.

SOX2 Overexpression Enhances Spheroid Formation and Promotes Dysplasia in TUM622 Acini.
SOX2 is amplified and/or overexpressed in the majority of LUSC patients and known as a lineage survival oncogene in the context of LUSC (4, 8, 33). Exactly how the high levels of SOX2 expression manifest at the tissue level during LUSC progression remains unclear. Since TUM622 cells express moderate levels of SOX2 in comparison with other LUSC cell lines (Fig. 4A; compare TUM622 Vector to LUSC lines), we reasoned that our 3D culture is uniquely suited for investigating the functional impact of SOX2 overexpression on LUSC progression.

We first generated stable pools of control Vector and SOX2-overexpressing TUM622 cells (termed Vector and SOX2oe cells) by transducing the parental TUM622 line with lentiviral vectors. In two dimensions, SOX2-overexpressing cells adopted a mesenchymal phenotype in comparison with round Vector cells (*SI Appendix*, Fig. S4A). Using qRT-PCR and Western blot, we confirmed that SOX2 is overexpressed in the SOX2oe cells (Fig. 4 A and B) but does not exceed the level found in a LUSC cell line with a highly amplified SOX2 locus (Fig. 4A; compare with H520). We then plated Vector and SOX2oe cells as previously described into 3D ECM and monitored their growth and morphology over time. Results showed that, at the end of a 2-wk culturing period, twice as many spheroids were formed in SOX2oe wells compared with Vector wells, indicating an enhanced self-renewal potential of the spheroid-forming population within TUM622 cells (Fig. 4C and *SI Appendix*, Fig. S4 B and C). However, the number of cells in SOX2oe spheroids only showed a 50-fold increase from day 5 to day 15, while Vector acini increased more than 200-fold, which is consistent with the corresponding changes in spheroid volume (Fig. 4D and *SI Appendix*, Fig. S4 C and D). Strikingly, these SOX2oe spheroids no longer retained the acinar-like morphology and were filled with cells in the center, similar to spheroids derived from other NSCLC cell lines examined (compare Figs. 1A and 4E). This dramatic change
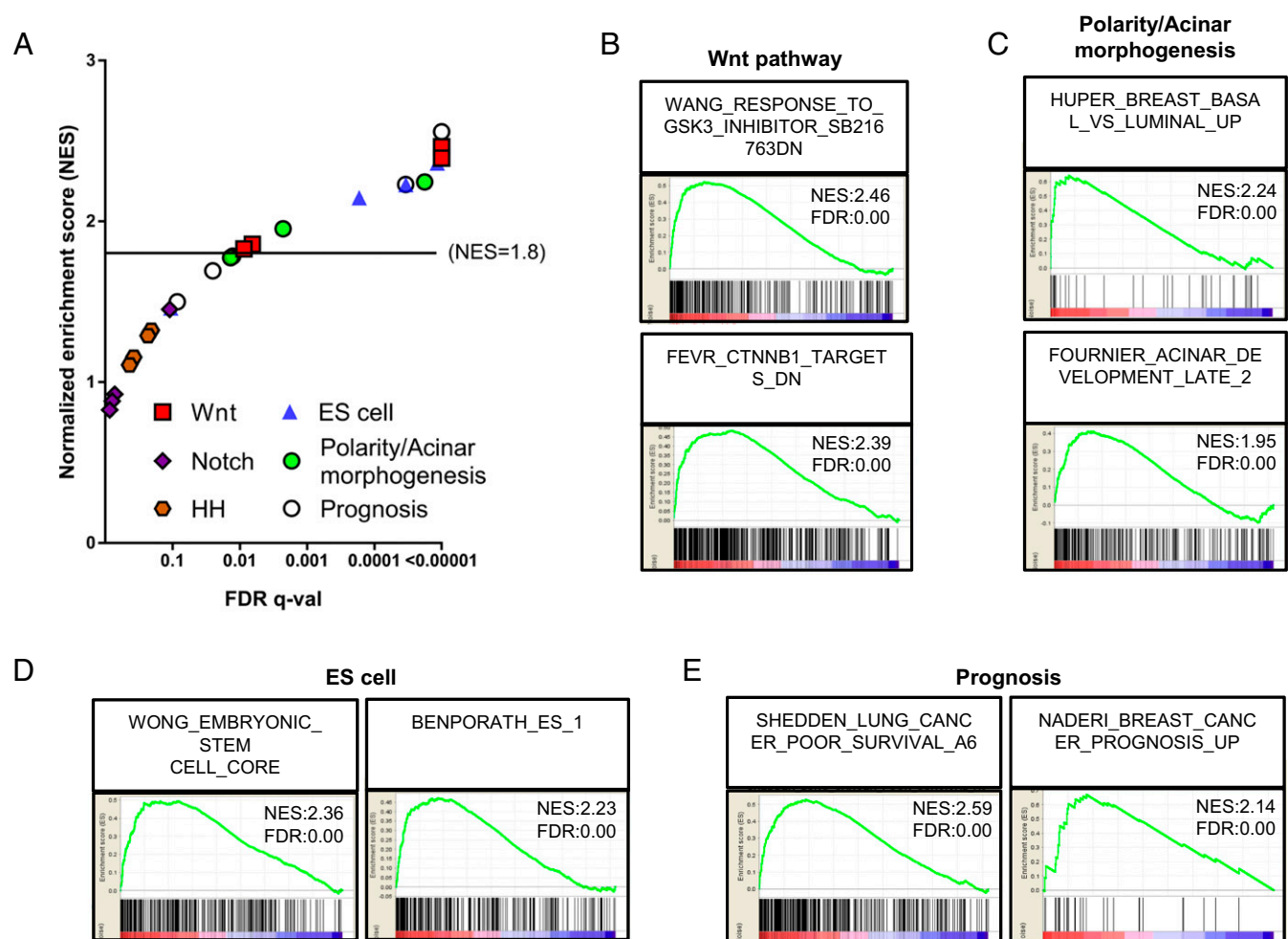
Fig. 3. Gene sets enriched in TUM622 3D vs. 2D culture. (*A*) Top four enriched gene sets identified from TUM622 3D culture (in comparison with TUM622 2D culture) that belong to each of the following categories: key signaling pathways (Wnt, Notch, and Hedgehog signaling), ES cell, polarity/acinar morphogenesis, and prognosis. Horizontal axis represents the −log[10] of FDR value, and the vertical axis represents NES. See the entire list of enriched gene sets corresponding to each category in Dataset S1. (*B–E*) Enrichment plots of the top two enriched gene sets in each of the categories represented in *A*.

in morphology led us to investigate whether cell polarity was affected as a consequence of SOX2 overexpression. A closer examination with immunofluorescent staining revealed an altered distribution of GM-130 from the apical side to a random localization within cells of SOX2oe spheroids, but basal polarity marker ITGA6 remains intact (Fig. 4*F*). SOX2 overexpression did not alter the localization pattern of β-catenin, E-cadherin, or Vimentin, which is consistent with the lack of invasive behavior of SOX2oe cells in three dimensions (Fig. 4*F*).

To understand how SOX2 overexpression may have contributed to the smaller spheroid size, we compared the proliferation, apoptosis, and differentiation capacity of Vector vs. SOX2oe cells in culture. Here, we found that, unlike Vector acini, cells in the center of the SOX2oe spheroids were able to survive without direct contact with the ECM (Fig. 4*E*). In agreement with this observation, qRT-PCR of Vector and SOX2oe mRNA harvested from 3D cultures showed an increase in the expression of antiapoptotic protein BCL-2 and a decrease of apoptosis-inducing FAS receptor (Fig. 4*G*). However, this decrease in apoptosis is also accompanied by an altered distribution in cell cycle stages (*SI Appendix*, Fig. S4*E*). In addition, SOX2 overexpression led to a decrease in Vimentin and an increase in involucrin (IVL) expression, indicating increased commitment to the squamous lineage (Fig. 4*G*). These changes may explain the reduced growth rate of SOX2oe spheroids.

Together, these data suggest that, in the context of TUM622 cells, further increasing the level of SOX2 expression enhanced spheroid formation but concomitantly drove dysplasia by disruption of apical–basal cell polarity, and reinforced commitment of cells to the squamous lineage.

CAFs Increase the Self-Renewal Potential and Invasiveness of TUM622 Acini. TUM622 cells are highly malignant, and the acini they form contain a mixture of cells analogous to intact tumors. When oncogenic SOX2 is overexpressed, the spheroids do not appear to be invasive when grown in 3D ECM. We reasoned that cell extrinsic components in the TME are required to broaden the plasticity of TUM622 acini and allow them to display a more aggressive, invasive phenotype. To test this hypothesis, we established a coculture system where CAFs are either overlaid or coembedded in the ECM containing TUM622 cells (Fig. 5*A*). These CAFs uniformly express alpha-smooth muscle actin and do not express CD31 or CD45, indicating a population of cells devoid of endothelial or hematopoietic contamination (*SI Appendix*, Fig. S5 *A* and *B*). Moreover, overlaid CAFs were able to aggregate into small foci within 48 h after plating, even though they were initially distributed evenly on top of the ECM (Fig. 5*A* and *SI Appendix*, Fig. S5*C*). When TUM622 cells were cocultured with CAFs, the frequency of cells that could form acini dramatically increased, as did their overall size (Fig. 5 *B* and *C*). Strikingly, acini that
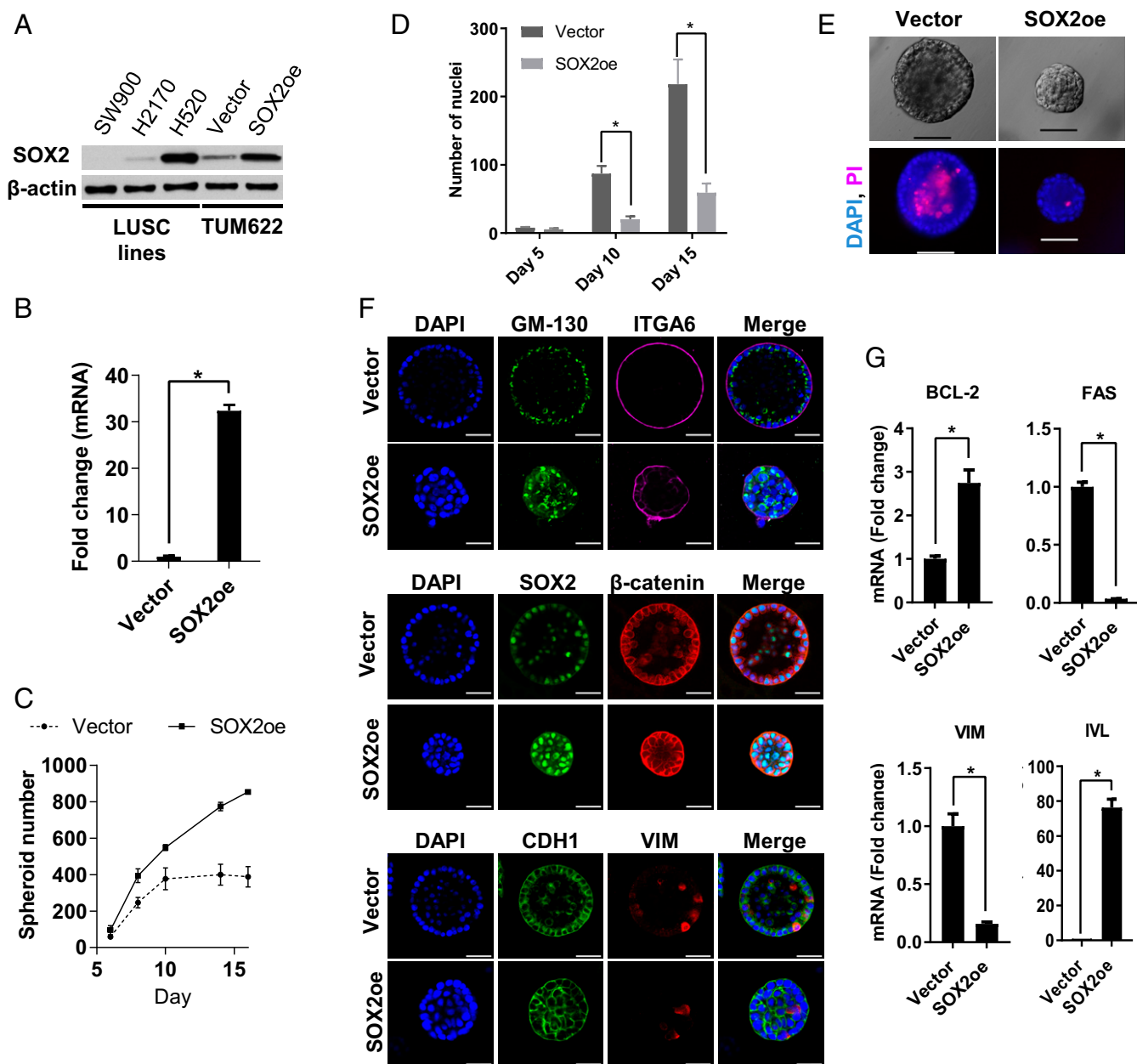
Fig. 4. SOX2 overexpression enhances the spheroid forming capacity of TUM622 cells and induces dysplasia. (*A*) Western blot comparing the expression level of SOX2 in Vector and SOX2oe cells to three LUSC cell lines with no/low (SW900), medium (H2170), and high (H520) levels of SOX2 expression. (*B*) *SOX2* expression level in Vector vs. SOX2oe spheroids in 3D culture as quantified by qRT-PCR. Column represents triplicates, and error bars represent SD; $P < 3 \times 10^{-5}$. (*C*) Quantification of the number of Vector and SOX2oe spheroids in 3D ECM from days 6 to 14 after initial seeding (15,000 per well). (*D*) Quantification of the number of nuclei in half of a Vector and SOX2oe spheroid at indicated time points ($n = 5$). Error bars represent SD. *$P < 0.05$ in Student's *t*-test. (*E*) SOX2 overexpression induced a hyperplastic to a dysplastic transition in spheroid phenotype. (*Top*) Bright-field images; (*Bottom*) corresponding fluorescent images of DAPI and propidium iodide (PI; dead cell) staining. (Scales bars, 100 μm.) (*F*) Comparison of immunofluorescent staining of Vector and SOX2oe spheroids with apical-basal cell polarity and cell-adhesion markers. (Scales bars, 50 μm.) (*G*) The qRT-PCR of *BCL-2*, *FAS*, *IVL*, and *VIM in* Vector vs. SOX2oe spheroids. Column represents triplicates, and error bars represent SD. *$P < 0.05$.

are in close proximity with CAFs invade the ECM, often forming "teardrop"-shaped structures (Fig. 5*D* and *SI Appendix*, Fig. S5 *C* and *D*). TUM622 cells at the invasive front point toward the CAFs and display a reduction in E-cadherin and ITGA6 expression, but are positive for Vimentin expression (Fig. 5 *D* and *E*). However, before invasion, some cells in TUM622 acini are already positive for Vimentin staining. Therefore, we could not determine whether cells at the leading front gained Vimentin expression during invasion or were already Vimentin-positive before invasion. Embedding CAFs together with TUM622 cells enhanced growth and

invasion of acinar-like structures as well (*SI Appendix*, Fig. S5C). Thus, by incorporating CAFs into our culture system, we were able to unveil greater plasticity of TUM622 cells and expanded our system to model not only cancer cell–ECM but also cancer cell–CAF interactions during tumorigenesis.

CAFs Suppress SOX2-Induced Dysplasia in Coculture. We then asked if CAFs could act synergistically with high levels of SOX2 to further enhance the self-renewal and invasiveness of spheroids in three dimensions. Here, we plated Vector and SOX2oe cells
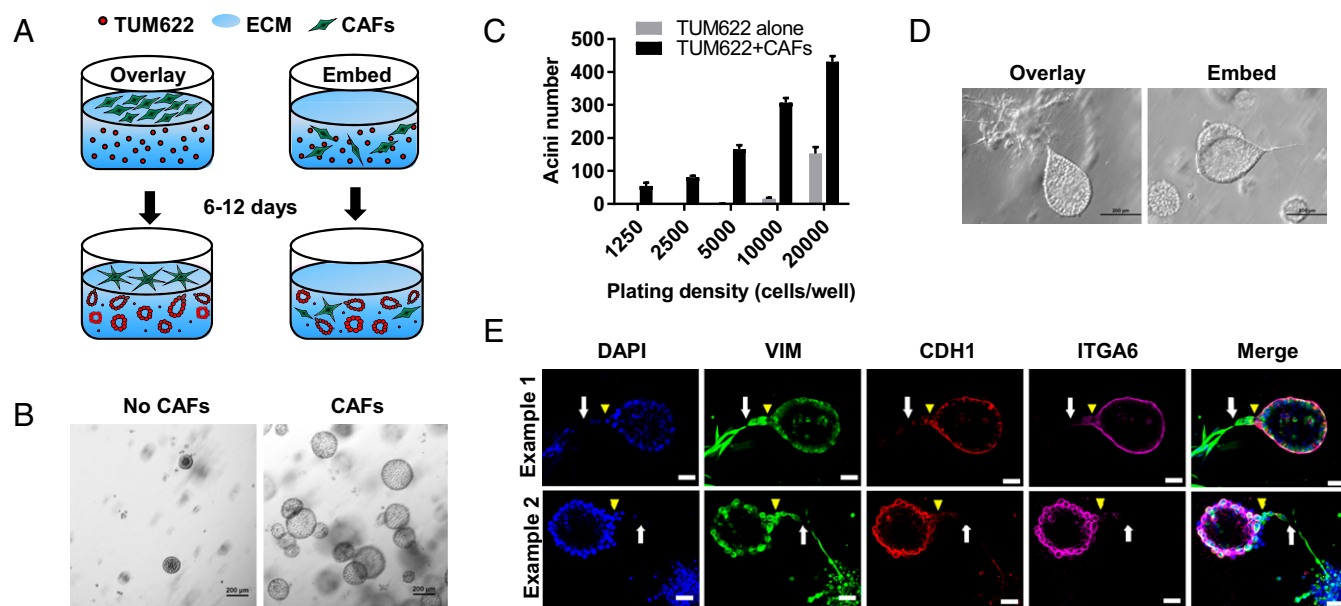
Fig. 5. CAFs increase the number and invasiveness of TUM622 acini. (*A*) Micrograph depicting coculture setups where CAFs are either overlaid or embedded together with TUM622 cells in ECM. After 6 d to 12 d in coculture, TUM622 cells are able to form more and larger acini compared with monoculture, and invade the ECM when in close proximity or direct contact with CAFs. (*B*) Bright-field images of TUM622 3D cultures in the presence or absence of overlaid CAFs after 8 d. (Scale bars, 200 μm.) (*C*) Quantification of acini number in monoculture vs. coculture. Columns represent the average of four replicates performed in technical triplicates, error bars represents SD, and $P < 2 \times 10^{-5}$. (*D*) Bright-field images showing teardrop-shaped acini forming in cocultures regardless of whether CAFs are overlaid or coembedded in the ECM. (Scale bars, 200 μm.) (*E*) Immunofluorescent staining of Vimentin (green), CDH1 (red), and ITGA6 (magenta) on TUM622 acini in coculture. White arrows point at the invading front where CAFs and epithelial cells make potential contacts. Yellow arrowheads denote points of evasion from the epithelial monolayer. (Scale bars, 50 μm.)

either as a monoculture or a coculture with CAFs and compared their growth and morphology over time. Data showed that, similar to TUM622 cells, adding CAFs further increased spheroid formation in both Vector and SOX2oe cultures by the end of a 2-wk culture period (Fig. 6*A*). However, we made the unexpected observation that many acinar-like structures were able to form in the SOX2oe and CAF cocultures (Fig. 6*B*), whereas almost all SOX2oe spheroids lacked hollow lumens in monocultures (*SI Appendix*, Fig. S6). Immunofluorescence further demonstrated that the SOX2oe acinar-like structures resemble Vector acini, with the typical monolayer of cells surrounding a hollow lumen (Fig. 6 *C* and *D*). Although SOX2oe acinar-like structures were able to form regardless of their distance from the CAFs, only those that were in close proximity to CAFs reduced E-cadherin and ITGA6 expression and became invasive (Fig. 6 *C* and *D*). Moreover, cells at the invading front were confirmed to be epithelial cells, as they expressed either the squamous marker p63 or SOX2 (Fig. 6 *C* and *D*). It is important to note that not all spheroids in SOX2oe wells form as hollow structures in the presence of CAFs, and some remain as spheroids without lumens. Nevertheless, the abundance of acinar-like structures in the SOX2oe CAF cocultures indicates that TUM622 still displays plasticity even when an oncogene such as SOX2 is overexpressed (Fig. 6*B* and *SI Appendix*, Fig. S6). These data suggest that CAFs could antagonize and even override high levels of oncogenic SOX2 to restore the formation of luminal structures and promote invasion.

Discussion

Cancer cell−TME interactions represent an important mechanism regulating tumorigenesis and have emerged as a promising target for the development of anticancer therapies (16). However, efforts in understanding this interaction have been hampered by lack of appropriate in vitro models that faithfully recapitulate human LUSC. Here, we report the establishment of

a 3D coculture that enables the investigation of how human LUSC cells interact with two major components of the TME, ECM and CAFs, in regulating the tumor phenotype. Using this system, we uncovered the capacity of LUSC cells to undergo phenotypic switches in response to changes in oncogene expression as well as TME composition. Significantly, our data establish that, in the context of LUSC, the TME can be dominant over the malignant genotype in dictating the disease phenotype. The capacity of our system to model LUSC progression in vitro while preserving the plasticity of malignant cells further distinguishes it from other in vitro LUSC models.

The ability to capture changes in tissue architecture during LUSC tumorigenesis is another key feature of our model. We have shown that a subpopulation of LUSC cells from a primary PDX-derived culture has the ability to undergo acinar morphogenesis when embedded in an ECM. The observation that these acini capture key features of normal epithelial architecture yet remain hyperproliferative indicates a phenotypic conversion to hyperplasia, the earliest stage of LUSC tumorigenesis (27). Since growth and tissue architecture are separable attributes in these acinar-like structures, we were able to further investigate how additional oncogenic insults and changes in TME contribute to loss of tissue architecture during LUSC tumorigenesis. This property fills an important gap in other 3D models that interpret tumorigenicity mainly based on the number and size of tumor spheroids formed (34–36).

Consistent with the highly organized tissue architecture of TUM622 acini, key signaling pathways and factors involved in normal lung development were up-regulated in 3D compared with 2D culture. This includes the transcription factor SOX2, which is highly amplified and/or overexpressed in the majority of LUSC patients (4). Due to its key role in pluripotent stem cells as well as lung progenitors (37, 38), overexpression of SOX2 has been widely speculated to contribute to carcinogenesis by inducing stem-like properties that underlie aggressive clinical
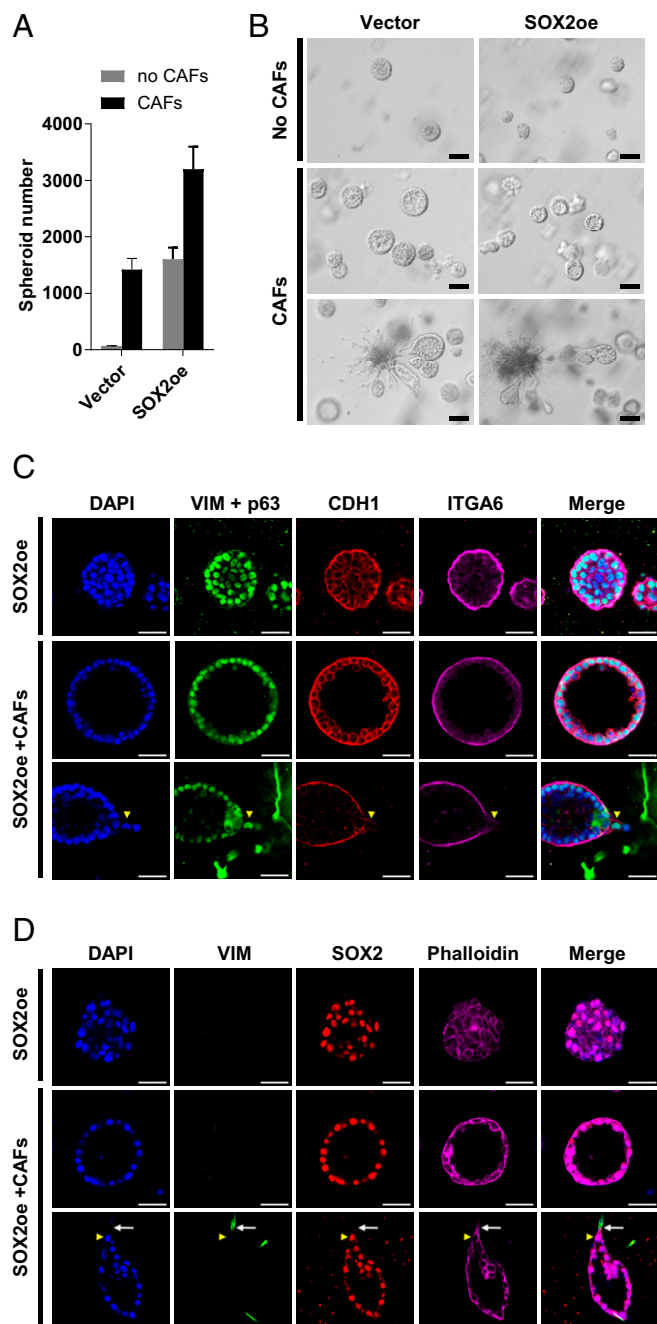
Fig. 6. CAFs enhance the acinar forming capacity of SOX2oe TUM622 cells and suppress dysplasia. (*A*) Quantification of spheroids formed from Vector and SOX2oe cells as monoculture/coculture with CAFs. Each column represents triplicates. Error bars represent SD. (*B*) CAFs induce the formation of acinar-like structures when in coculture with SOX2oe cells. Both Vector and SOX2oe spheroids become invasive when they are in close proximity with CAFs. (Scales bars, 100 μm.) (*C*) Immunofluorescence of SOX2oe monoculture as well as CAF cocultures stained for Vimentin (cytoplasmic)/p63 (nuclear), E-Cadherin, and ITGA6. Anti-vimentin and anti-p63 antibodies were stained with the same secondary antibody (green). (*D*) Immunofluorescence of SOX2oe monoculture as well as CAF cocultures stained for Vimentin, SOX2, and Phalloidin. (Scale bars, 50 μm.)

behavior and poor differentiation status (39–41). Indeed, within our culture, the small subpopulation of AFCs displays stem-like characteristics, being able to self-renew and give rise to diverse progenies. However, this hypothesis would not explain the

preferential amplification of SOX2 in LUSC as opposed to LUAD as well as the correlation of high SOX2 level with a better prognosis in several studies of human LUSC (42, 43). To elucidate the paradoxical roles of SOX2 in simultaneously promoting stemness and better prognosis in LUSC requires a better understanding of the functional impact of SOX2 overexpression at the tissue level.

Using our system, we provide direct evidence that overexpression of SOX2 is sufficient to drive a dysplastic phenotype in LUSC cells in vitro, where disorganized solid spheroids instead of acinar-like structures are formed. This is consistent with previous studies showing that SOX2 amplification is an early event during LUSC tumorigenesis and correlates with the progression between low- and high-grade dysplasia in vivo (10, 44). While this manuscript was in preparation, another study reported the role of SOX2 in driving dysplasia in an air–liquid interface culture modeling the earliest stages of bronchial epithelial carcinogenesis, further supporting our observations (45). Notably, while SOX2oe spheroids are dysplastic, they are not invasive, indicating that dysplasia does not necessarily lead to an invasive behavior in LUSC cells. Closer examination of the dysplastic spheroids revealed SOX2 as a master regulator that affects multiple aspects of LUSC cell biology, including apical–basal cell polarity, survival, proliferation, apoptosis, and differentiation. Importantly, SOX2 was shown to be able to enhance self-renewal and survival by suppressing apoptosis, while promoting commitment and differentiation of cells to the squamous lineage. These observations are in agreement with a recent publication showing that, although associated with an ES-like signature, SOX2 overlaps broadly with squamous lineage factor p63 in genome-wide occupancy in LUSC cells (46). Together, these data suggest that SOX2 is pleiotropic in the context of LUSC and provide a possible explanation for why SOX2 increased spheroid formation but simultaneously reduced their growth in our culture system. However, this raises the question of how LUSC cells maintain the balance between these seemingly counterproductive roles of SOX2 during tumorigenesis.

Our data suggest that this balance between growth and differentiation is determined by the TME. This is most prominently demonstrated by the addition of CAFs to our culture. CAFs have been shown to promote growth and invasion in various cancer types by secreting protumorigenic factors as well as through remodeling the ECM (47). Consistently, CAFs increased both the frequency and sizes of TUM622 acini in our culture. When in close proximity, CAFs induced TUM622 acini to become invasive. Strikingly, CAFs could suppress SOX2-induced dysplasia and restore acinar-like structures in coculture. In these cocultures, the acinar tissue architecture is restored, and the balance between growth and differentiation is readjusted to favor growth. Although the exact mechanism by which these cells develop as acinar-like structures is still under investigation, it is possible that this attribute could be dependent, at least in part, on paracrine factors produced during the reciprocal interactions of tumor epithelial cells and CAFs. These paracrine factors most likely affect signaling pathways downstream of SOX2 but not directly on SOX2 transcription, as the transgenic SOX2 expression is regulated by a constitutively active CMV promoter. Alternatively, CAFs could indirectly modulate tumor architecture through changing the biochemical and biomechanical properties of the ECM that lead to altered ECM receptor signaling (48). It is important to note that not all spheroids in SOX2oe cocultures become hollow, and some remain as spheroids without lumens. However, due to the highly heterogeneous nature of the culture, it remains technically challenging to determine whether the appearance of acinar-like structures occurred by reversion or selection. Nevertheless, the observation that acinar-like structures could form from TUM622 cells with high SOX2 levels (Fig. 6*C*) suggests that their cellular plasticity is retained regardless of this oncogenic change. Combined with the earlier observation that malignant TUM622 could be reverted to display
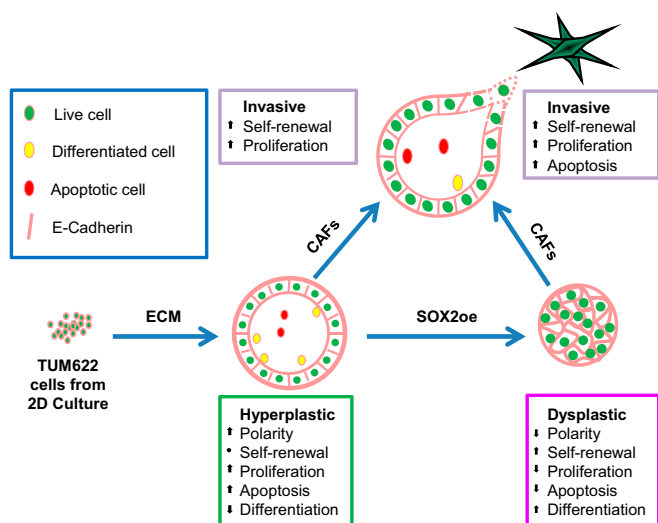
Fig. 7. TME is dominant over the genotype in determining the epithelial architecture of TUM622 cells in vitro. A subpopulation of TUM622 cells has the ability to form acinar-like structures when plated as single cells in ECM culture. These acini are hyperplastic but nevertheless display proper apical–basal cell polarity, similar to hyperplasia observed at the earliest stage of LUSC development. Overexpression of SOX2 in TUM622 cells increases spheroid-forming capacity of TUM622 cells and drives a hyperplastic to dysplastic change in acinar phenotype where apical–basal cell polarity is disrupted and solid spheroids are formed. SOX2oe spheroids also display reduced apoptosis and increased differentiation. Addition of CAFs to TUM622 3D culture enhances acinar formation/growth and promotes invasion toward the CAFs. CAFs could promote the formation of an acinar-like structure in SOX2oe spheroids and induce invasion. Therefore, the key stages of LUSC development, from hyperplasia to dysplasia and eventually invasion, can be observed in this model system.

acinar-like phenotypes in an acellular TME, our data confirm a key concept formulated more than two decades ago by the Bissell laboratory and others that posits cancer cells are highly plastic and the TME may powerfully override the malignant genotypes to various degrees by normalizing the phenotype and function of cancer cells (49).

In summary, we uncovered a previously unappreciated plasticity of LUSC cells by using a coculture of LUSC with CAFs. We showed that, although oncogenic changes may play important roles in driving tumorigenesis, the final phenotypic output is determined by the interaction between the oncogenic changes and the surrounding microenvironment. Importantly, we demonstrated that LUSC tumor architecture is plastic and sensitive to changes in the TME, including the ECM and CAFs. These changes modulate the balance between growth and differentiation of tumor cells but also determine their invasiveness (Fig. 7). These findings indicate that, in addition to direct targeting of tumor cells, the signaling network between the TME and cancer cells could represent the basis of new, more effective treatments. Future studies can use this platform to further elucidate the specific signaling pathways and molecular mechanisms that mediate these reciprocal interactions.

Materials and Methods

Cell Culture and Cells. Human lung tumor tissues were obtained from Asterand in accordance with appropriate consent procedures. Tumor tissues were processed as previously described (28) for the establishment of cancer cell lines and CAFs. The TUM622 and TUM110 were generated from patients with LUSC, TUM426 was generated from a patient with bronchioloalveolar carcinoma, and TUM449 was generated from a patient with LUAD. These patient-derived cell lines were maintained in SF bronchial epithelial cell growth medium (catalog #CC-3170; Lonza), which was changed 50% every other day. CAF culture was established and maintained in Roswell Park Memorial Institute (RPMI) medium with 20% FBS. Human primary lung epithelial cells BEAS-2B (ATCC) and NHBE (Lonza) were maintained according to manufacturer's protocol. Cell lines NCI-H520 and HCC2935 were procured from ATCC and grown in RPMI media supplemented with 2 mM L-glutamine, 50 units per milliliter of penicillin, 50 μg/mL of streptomycin, and 10% FBS.

Morphogenesis Assay and CAF Coculture. Morphogenesis assays were performed by mixing cells with ECM (BD Biosciences Matrigel catalog #356231 or Trevigen Cultrex catalog #3443-005-01) on ice, plated in triplicate into 24-well tissue culture plates, and incubated at 37 °C and 5% CO_2. After solidification for 30 min, culture media was added. For coculture experiments, CAFs were either overlaid on top of solidified Cultrex matrix or coembedded with TUM622 at the time of plating at a ratio of 2:1. Cultures were kept for 8 d to 12 d, with media replaced every 2 d. Serial passaging of TUM622 acini was performed by extracting acini (day 10) from the ECM via Cultrex 3D-cell harvesting kit (catalog #3448-020-K; Trevigen) according to manufacturer's recommendation. Acini were made into a single-cell suspension with trypsin (catalog #CC-5034; Lonza) and replated as described above. Inhibition of Notch and Wnt signaling pathway in 3D cultures was performed with small-molecule inhibitors/agonist IWR-1 (catalog #681669; EMD Millipore), CHIR-99021 (catalog #SML1046; Sigma) and DBZ (catalog #4489; Tocris) at the indicated concentrations. Media containing inhibitors/agonists were replaced once every 2 d for 10 d. The number and size of acini/spheroids were quantified with GelCount (Oxford Optronix, Inc.).

Microarray and GSEA Analysis. TUM622 cells from 2D and 3D cultures were harvested by direct trypsinization or acini extraction (as previously described) followed by trypsinization. Single-cell suspensions were then stained with DAPI, EpCAM (catalog #347198; BD Bioscience) or control IgG antibody and subjected to FACS sorting using a BD FACSAria II to obtain live, EpCAM+ epithelial cell populations. Each condition was performed in triplicate. RNA from TUM622 cells (2D or 3D) was isolated using the RNEasy kit (catalog #74104; Qiagen). The cDNA synthesis and subsequent in vitro antisense RNA (cRNA) amplification and biotin labeling were performed as described by the manufacturer. For each sample, 10 μg of biotin-labeled cRNA was fragmented and hybridized to Human Genome U133+2 GeneChip oligonucleotide arrays (Affymetrix) using buffers and conditions recommended by the manufacturer. GeneChips were then washed and stained with Streptavidin R-phycoerythrin (Molecular Probes) using the Gene-Chip Fluidics Station 450, and scanned with an Affymetrix GeneChip Scanner 3000. The gene expression data were processed by guanine cytosine robust multiarray average algorithm. Probe sets were filtered to obtain robustly expressed qualifiers (average signal value of ≥50, 100% present call in any of the sample group). GSEA was conducted using GSEA software (Broad Institute). Gene sets related to key signaling pathways including canonical Wnt signaling, Notch, and Hedgehog pathway, ES cell factors, and cell polarity/acinar morphogenesis were curated for identification of gene sets that are significantly enriched [normalized enrichment score (NES) > 1.8, FDR q value < 0.05].

1. Boström H, et al. (1996) PDGF-A signaling is a critical event in lung alveolar myofibroblast development and alveogenesis. *Cell* 85:863–873.
2. Morrisey EE, Hogan BL (2010) Preparing for the first breath: Genetic and cellular mechanisms in lung development. *Dev Cell* 18:8–23.
3. Herriges M, Morrisey EE (2014) Lung development: Orchestrating the generation and regeneration of a complex organ. *Development* 141:502–513.
4. Bass AJ, et al. (2009) SOX2 is an amplified lineage-survival oncogene in lung and esophageal squamous cell carcinomas. *Nat Genet* 41:1238–1242.
5. Justilien V, et al. (2014) The PRKCI and SOX2 oncogenes are coamplified and cooperate to activate Hedgehog signaling in lung squamous cell carcinoma. *Cancer Cell* 25:139–151.
6. Wang NJ, et al. (2011) Loss-of-function mutations in Notch receptors in cutaneous and lung squamous cell carcinoma. *Proc Natl Acad Sci USA* 108:17761–17766.

CELL BIOLOGY

7. Jemal A, et al. (2011) Global cancer statistics. *CA Cancer J Clin* 61:69–90.
8. Cancer Genome Atlas Research Network (2012) Comprehensive genomic characterization of squamous cell lung cancers. *Nature* 489:519–525.
9. Siegel R, Naishadham D, Jemal A (2013) Cancer statistics, 2013. *CA Cancer J Clin* 63:11–30.
10. Jamal-Hanjani M, et al.; TRACERx Consortium (2017) Tracking the evolution of non-small-cell lung cancer. *N Engl J Med* 376:2109–2121.
11. Tanaka H, et al. (2007) Lineage-specific dependency of lung adenocarcinomas on the lung development regulator TTF-1. *Cancer Res* 67:6007–6011.
12. Incardona F, et al.; Reproducibility Project: Cancer Biology (2015) Registered report: Interactions between cancer stem cells and their niche govern metastatic colonization. *eLife* 4:e06938.
13. Quail DF, Joyce JA (2013) Microenvironmental regulation of tumor progression and metastasis. *Nat Med* 19:1423–1437.
14. Shimosato Y, et al. (1980) Prognostic implications of fibrotic focus (scar) in small peripheral lung cancers. *Am J Surg Pathol* 4:365–373.
15. Gaggioli C, et al. (2007) Fibroblast-led collective invasion of carcinoma cells with differing roles for RhoGTPases in leading and following cells. *Nat Cell Biol* 9:1392–1400.
16. Gascard P, Tlsty TD (2016) Carcinoma-associated fibroblasts: Orchestrating the composition of malignancy. *Genes Dev* 30:1002–1019.
17. Kalluri R, Zeisberg M (2006) Fibroblasts in cancer. *Nat Rev Cancer* 6:392–401.
18. Kojima Y, et al. (2010) Autocrine TGF-beta and stromal cell-derived factor-1 (SDF-1) signaling drives the evolution of tumor-promoting mammary stromal myofibroblasts. *Proc Natl Acad Sci USA* 107:20009–20014.
19. Petersen OW, Rønnov-Jessen L, Howlett AR, Bissell MJ (1992) Interaction with basement membrane serves to rapidly distinguish growth and differentiation pattern of normal and malignant human breast epithelial cells. *Proc Natl Acad Sci USA* 89:9064–9068.
20. Schmeichel KL, Bissell MJ (2003) Modeling tissue-specific signaling and organ function in three dimensions. *J Cell Sci* 116:2377–2388.
21. Debnath J, Brugge JS (2005) Modelling glandular epithelial cancers in three-dimensional cultures. *Nat Rev Cancer* 5:675–688.
22. Jechlinger M, Podsypanina K, Varmus H (2009) Regulation of transgenes in three-dimensional cultures of primary mouse mammary cells demonstrates oncogene dependence and identifies cells that survive deinduction. *Genes Dev* 23:1677–1688.
23. Weaver VM, et al. (1997) Reversion of the malignant phenotype of human breast cells in three-dimensional culture and in vivo by integrin blocking antibodies. *J Cell Biol* 137:231–245.
24. Wu X, Peters-Hall JR, Bose S, Peña MT, Rose MC (2011) Human bronchial epithelial cells differentiate to 3D glandular acini on basement membrane matrix. *Am J Respir Cell Mol Biol* 44:914–921.
25. Sasai K, et al. (2011) Oncogene-mediated human lung epithelial cell transformation produces adenocarcinoma phenotypes in vivo. *Cancer Res* 71:2541–2549.
26. Sato M, et al. (2006) Multiple oncogenic changes (K-RAS(V12), p53 knockdown, mutant EGFRs, p16 bypass, telomerase) are not sufficient to confer a full malignant phenotype on human bronchial epithelial cells. *Cancer Res* 66:2116–2128.
27. Saccomanno G, Archer VE, Auerbach O, Saunders RP, Brennan LM (1974) Development of carcinoma of the lung as reflected in exfoliated cells. *Cancer* 33:256–270.
28. Damelin M, et al. (2011) Delineation of a cellular hierarchy in lung cancer reveals an oncofetal antigen expressed on tumor-initiating cells. *Cancer Res* 71:4236–4246.
29. Geles KG, et al. (2016) Upregulation of RNA processing factors in poorly differentiated lung cancer cells. *Transl Oncol* 9:89–98.
30. Dann SG, et al. (2015) Reciprocal regulation of amino acid import and epigenetic state through Lat1 and EZH2. *EMBO J* 34:1773–1785.
31. Fazekas de St G; Fazekas de St Groth (1982) The evaluation of limiting dilution assays. *J Immunol Methods* 49:R11–R23.
32. Hu Y, Smyth GK (2009) ELDA: Extreme limiting dilution analysis for comparing depleted and enriched populations in stem cell and other assays. *J Immunol Methods* 347:70–78.
33. Hussenet T, et al. (2010) SOX2 is an oncogene activated by recurrent 3q26.3 amplifications in human lung squamous cell carcinomas. *PLoS One* 5:e8960.
34. Majety M, Pradel LP, Gies M, Ries CH (2015) Fibroblasts influence survival and therapeutic response in a 3D co-culture model. *PLoS One* 10:e0127948.
35. Amann A, et al. (2014) Development of an innovative 3D cell culture system to study tumour–Stroma interactions in non-small cell lung cancer cells. *PLoS One* 9:e92511.
36. Ekert JE, et al. (2014) Three-dimensional lung tumor microenvironment modulates therapeutic compound responsiveness in vitro–Implication for drug development. *PLoS One* 9:e92248.
37. Takahashi K, Yamanaka S (2006) Induction of pluripotent stem cells from mouse embryonic and adult fibroblast cultures by defined factors. *Cell* 126:663–676.
38. Que J, Luo X, Schwartz RJ, Hogan BLM (2009) Multiple roles for Sox2 in the developing and adult mouse trachea. *Development* 136:1899–1907.
39. Ben-Porath I, et al. (2008) An embryonic stem cell-like gene expression signature in poorly differentiated aggressive human tumors. *Nat Genet* 40:499–507.
40. Jia X, et al. (2011) SOX2 promotes tumorigenesis and increases the anti-apoptotic property of human prostate cancer cell. *J Mol Cell Biol* 3:230–238.
41. Alonso MM, et al. (2011) Genetic and epigenetic modifications of Sox2 contribute to the invasive phenotype of malignant gliomas. *PLoS One* 6:e26740.
42. Wilbertz T, et al. (2011) SOX2 gene amplification and protein overexpression are associated with better outcome in squamous cell lung cancer. *Mod Pathol* 24:944–953.
43. Brcic L, et al. (2012) Morphologic and clinicopathologic features of lung squamous cell carcinomas expressing Sox2. *Am J Clin Pathol* 138:712–718.
44. McCaughan F, et al. (2010) Progressive 3q amplification consistently targets SOX2 in preinvasive squamous lung cancer. *Am J Respir Crit Care Med* 182:83–91.
45. Correia LL, et al. (2017) SOX2 drives bronchial dysplasia in a novel organotypic model of early human squamous lung cancer. *Am J Respir Crit Care Med* 195:1494–1508.
46. Watanabe H, et al. (2014) SOX2 and p63 colocalize at genetic loci in squamous cell carcinomas. *J Clin Invest* 124:1636–1645.
47. Kalluri R (2016) The biology and function of fibroblasts in cancer. *Nat Rev Cancer* 16:582–598.
48. Northey JJ, Przybyla L, Weaver VM (2017) Tissue force programs cell fate and tumor aggression. *Cancer Discov* 7:1224–1237.
49. Bissell MJ, Radisky DC, Rizki A, Weaver VM, Petersen OW (2002) The organizing principle: microenvironmental influences in the normal and malignant breast. *Differentiation* 70:537–546.